

# Radio Continuum Observations of the Galactic Center: Photoevaporative Proplyd-like Objects near Sgr A\*

F. Yusef-Zadeh<sup>1</sup>, D. A. Roberts<sup>1</sup>, M. Wardle<sup>2</sup>, W. Cotton<sup>3</sup>, R. Schödel<sup>4</sup> & M. J. Royster<sup>1</sup>

<sup>1</sup>*Department of Physics and Astronomy and CIERA, Northwestern University, Evanston, IL 60208*

<sup>2</sup>*Department of Physics and Astronomy, Macquarie University, Sydney NSW 2109, Australia*

<sup>3</sup>*National Radio Astronomy Observatory, Charlottesville, VA 22903*

<sup>4</sup>*Instituto de Astfísica de Andalucía (CSIC), Glorieta de la Astronomía S/N, 18008 Granada, Spain*

## ABSTRACT

We present radio images within 30'' of Sgr A\* based on recent VLA observations at 34 GHz with 7.8  $\mu$ Jy sensitivity and resolution  $\sim 88 \times 46$  milliarcseconds (mas). We report 44 partially resolved compact sources clustered in two regions in the E arm of ionized gas that orbits Sgr A\*. These sources have size scales ranging between  $\sim 50$  and 200 mas (400 to 1600 AUs), and a bow-shock appearance facing the direction of Sgr A\*. Unlike the bow-shock sources previously identified in the near-IR but associated with massive stars, these 34 GHz sources do not appear to have near-IR counterparts at 3.8  $\mu$ m. We interpret these sources as a candidate population of photoevaporative protoplanetary disks (proplyds) that are associated with newly formed low mass stars with mass loss rates  $\sim 10^{-7} - 10^{-6} M_{\odot} \text{ yr}^{-1}$  and are located at the edge of a molecular cloud outlined by ionized gas. The disks are externally illuminated by strong Lyman continuum radiation from the  $\sim 100$  OB and WR massive stars distributed within 10'' of Sgr A\*. The presence of proplyds implies current in-situ star formation activity near Sgr A\* and opens a window for the first time to study low mass star, planetary and brown dwarf formations near a supermassive black hole.

*Subject headings:* Galaxy: center - clouds - ISM: general - ISM - radio continuum - stars: formation - protostars

## 1. Introduction

The Galactic center hosts a young population of stars centered on the strong radio source Sgr A\* which coincides with a  $4 \times 10^6 M_{\odot}$  black hole (Reid and Brunthaler 2004; Ghez et al. 2008; Gillessen et al. 2009). The young stellar cluster lies within 1 and  $10''$  (0.039–0.39 pc) of Sgr A\* and consists of about one hundred young massive OB and WR stars (Paumard et al. 2006; Lu et al. 2009).

The region within  $20''$  of Sgr A\* shows a number of infrared excess sources (Viehmann et al. 2006; Muzic et al. 2008; Eckart et al. 2013). Some of these dusty sources are hot, young stars interacting with the interstellar medium and creating bow-shock structures. Another group of infrared excess stars have partially resolved radio continuum counterparts and are interpreted as massive young stellar objects (YSOs) irradiated by the strong UV emission from the central stellar cluster (Yusef-Zadeh et al. 2014). Another indicator of star formation is the SiO (5-4) line emission from a dozen unresolved sources within 0.5 pc of Sgr A\* (Yusef-Zadeh et al. 2013). These may be highly embedded protostellar outflows, signifying an early phase of star formation near Sgr A\* in the last  $10^4 - 10^5$  years (Yusef-Zadeh et al. 2013).

A number of recent studies support in-situ star formation near Sgr A\* as the origin of massive stars in the last few million years (e.g., Genzel et al. 2010). In the disk of the Galaxy, circumstellar disks associated with low mass stars are expected to survive their hostile massive star formation environments. A number of circumstellar disks associated with low mass stars show cometary appearance and have been identified as proplyds (protoplanetary disks) in young star forming regions such as the Orion Nebula Cluster (ONC; O’Dell & Wen 1994), Carina Nebula (Smith et al. 2005) and the Trifid Nebula (Yusef-Zadeh et al. 2005). The proplyds of the ONC are photoevaporated and photoionized by the UV radiation from  $\theta^1$  Ori C and generally exhibit bow shock structures (Johnstone, Hollenback & Bally 1998; Störzer & Hollenbach 1998).

We present radio continuum observations within  $30''$  of Sgr A\* and report the detection of 44 radio continuum sources in 2 groupings  $15''$  and  $20''$  NE of Sgr A\*. Our 34 GHz observations reveal partially resolved sources with typical sizes of a few hundred AU at the 8 kpc distance to the Galactic center. In analogy with the proplyds found in the ONC, we interpret these radio continuum sources as proplyd candidates that are photoionized and photoevaporated by the radiation emitted by massive OB and WR stars near Sgr A\*. The upper limits to the infrared flux from the Galactic center proplyd candidates are consistent with gaseous disks orbiting low mass stars at a projected distance of 0.6 – 0.8 pc from Sgr A\*.

## 2. Observations and Data Reduction

Radio continuum observations were carried out with the Karl G. Jansky Very Large Array (VLA)<sup>1</sup> in its A-configuration at 34.5 GHz on March 9, 2014 (14A-232). We observed a

---

<sup>1</sup>Karl G. Jansky Very Large Array (VLA) of the National Radio Astronomy Observatory is a facility of the National Science Foundation, operated under a cooperative agreement by Associated Universities, Inc.

field of view with a radius of  $39''$  centered on Sgr A\* in Ka-band (8.7 mm) using the 3-bit sampler system, which provided full polarization correlations in 4 basebands, each 2 GHz wide, centered at 31.5, 33.5, 35.5 and 37.5 GHz. Each baseband was composed of 16 subbands 128 MHz wide. Each subband was comprised of 64 channels, each 2 MHz wide. We used 3C286 to calibrate the flux density scale and used both 3C286 and J1733-1304 (aka NRAO530) to calibrate the bandpass. We used J1744-3116 to calibrate the complex gains. The constructed image is of the  $30''$  surrounding Sgr A\* and has a spatial resolution of  $\sim 88 \times 46$  milliarcseconds (mas) (PA=  $-1.6^\circ$ ) and dynamic range  $\sim 2.2 \times 10^5$ . Using the large 8 GHz band, the  $1\sigma$  rms sensitivity is  $7.8 \mu\text{Jy}$ , which is a significant improvement over older observations which had only 100 MHz of bandwidth.

L'-band ( $3.8 \mu\text{m}$ ) data were taken with the Nasmyth Adaptive Optics System (NACO) at the Very Large Telescope (VLT; program 089.B-0503(B)) between June 26 and September 6, 2012 with the NACO L27 camera (pixel scale  $27 \text{ mas pixel}^{-1}$ ). A mosaic of about  $50'' \times 50''$  size was constructed using five pointings with total exposure time ranging between  $\sim 3000$  and 5500s. The images were reduced with the speckle holography method, as described in detail in Schödel et al. (2010, 2013).

We also present an SiO (5-4) spectrum derived from Atacama Large Millimeter Array (ALMA) observations carried out by the Science Verification team. Details of these observations are given in Yusef-Zadeh et al. (2013).

### 3. Results

Figure 1a shows a  $35'' \times 23''$  region of ionized gas associated with the E and N arms of Sgr A West, the mini-spiral HII region at 34 GHz. This spectacular image reveals a variety of new compact and diffuse sources: radio counterparts to near-IR identified massive stars such as IRS 16NE (Yusef-Zadeh et al. 2014), a ridge of blob-like structures arising from Sgr A\* extending toward the SW (Yusef-Zadeh et al. 2013), a spherical shell-like structure surrounding the M2 supergiant star IRS 7 (Serabyn et al. 1991), radio emission from the dusty AGB star IRS 3 (Pott et al. 2005) or from an embedded WR star (Horribin et al. 2004), the magnetar SGR J1745-29 (Kennea et al. 2013) and a large number of isolated and clustered compact HII regions.

We focus on the two concentrations of partially resolved sources denoted RC1 and RC2, which appear to be associated with the E arm of the mini-spiral HII region. Figure 1b shows the region in the E arm where 44 radio sources are detected. Figure 1c shows labeled sources P1–P44. The brightest sources, with peak flux densities ranging between 31 and  $482 \mu\text{Jy}$ , are mainly distributed in RC1 within a  $8'' \times 5''$  region of the E arm, centered roughly  $15.2''$  ( $0.61 \text{ pc}$ ) NE of Sgr A\* at a position angle of  $82 \pm 8^\circ$ . There are also weaker sources in RC2, P40–P44, with peak flux densities ranging between 34 to  $53 \mu\text{Jy}$  and centered  $\sim 20''$  from Sgr A\*. The 34 GHz integrated flux densities of these partially resolved compact sources range between 29 and  $1340 \mu\text{Jy}$  per  $88 \times 44 \text{ mas}$  beam. We note that the E arm in Figure 1a consists of two elongated ionized structures running parallel to each other forming an elliptical loop-like structure. The collection of radio sources are mainly found on the northern edge of the

E arm. Table 1 gives the ID number of 44 detected radio sources (P1–P44) coordinates, offsets from Sgr A\* in increasing angular distance, the total positional accuracy, peak and integrated fluxes at 34 GHz in Columns 1 to 7, respectively.

To illustrate the morphology of the newly resolved radio sources, Figure 2a shows the region of the highest concentration of proplyd candidates RC1. Almost all the sources have bow shock or elongated structures. Images of two candidates, P26 and P8 (Table 1), are presented in Figure 2b,c, respectively. Typical widths of bow-shock structures are  $\sim 45$  mas and the apices of the emission from the bow shocks are  $\sim 100$  mas corresponding to  $\sim 800$  AU. The bows point to within a few arcseconds of Sgr A\* where young massive stars are concentrated. This morphology strongly suggests that the resolved sources are externally illuminated by the central cluster of massive stars. The diffuse emission from the southern edge of the E arm (Fig. 1a) has a similar appearance suggesting that the massive stars are responsible for ionizing both the diffuse and compact sources in Sgr A West. The bow shock sources in the diffuse E arm are evaporating gaseous globule (EGG) candidates (see Fig. 1a) after Hester et al. (1996) and are an order of magnitude larger than those in RC1 and RC2.

The newly detected radio sources in the Galactic center show similar morphologies to the proplyds found in star forming regions in the Galaxy. Radio continuum observations of M42 in Orion first detected free-free emission from resolved sources with electron densities of  $\sim 10^6 \text{ cm}^{-3}$  (Churchwell et al. 1987; Garay, Moran & Reid 1987). HST observations of these sources, dubbed proplyds, showed cometary structures with bright heads pointing toward  $\theta^1$  Ori C (O’Dell & Wen 1994). We interpret the ionized gas in P1–P44 as arising from photoevaporated circumstellar disks that are photoionized by strong sources of UV radiation in the direction of Sgr A\*. The nuclear wind from the cluster of massive stars within few arcseconds of Sgr A\* could also contribute to the asymmetric shape of these proplyd candidates (Serabyn et al. 1991). The EUV Lyman continuum ionization radiation from massive stars is estimated to be  $\Phi \approx 2.5 \times 10^{50} \text{ s}^{-1}$  (Genzel, Hollenbach & Townes 1994) and for an assumed  $\sim 1$  pc distance from the source of ionization, the incident ionizing photon flux is  $\Phi/(4\pi (1 \text{ pc})^2) \approx 2 \times 10^{12} \text{ s}^{-1} \text{ cm}^{-2}$ . This is similar to that in Orion where the proplyds in M42 are located  $\sim 4 \times 10^{17} \text{ cm}$  from  $\theta^1$  Ori C with  $\Phi \approx 10^{49} \text{ s}^{-1}$ . Furthermore, the brightest sources in RC1 are closest to the central cluster and the typical peak flux density of radio sources in RC1 is stronger than that of RC2. This is consistent with the suggestion that both RC1 and RC2 are photoionized by the same stellar cluster near Sgr A\* and that RC1 is physically closer to Sgr A\* than RC2.

Assuming a spherical source with solid angle corresponding to a radius of 500 AU and electron density filling the sphere with volume filling factor of 1, the total mass of ionized gas  $M_i$  and the electron density are estimated to be  $2.5 \times 10^{-4} M_\odot$  and  $1.2 \times 10^5 \text{ cm}^{-3}$ , respectively. The electron density increases if we use a flattened geometry for the shape of ionized sources and a smaller volume filling factor. Assuming that the ionized gas expands at the sound speed ( $c_s \approx 10 \text{ km s}^{-1}$  for  $T = 8000 \text{ K}$ ), the mass-loss rates due to photoevaporation for sources with flux densities between 0.1 and 1 mJy are  $M_i/(r/c_s) \approx 10^{-7} - 10^{-6} M_\odot \text{ yr}^{-1}$ , respectively, where  $r$  is the radius of the disk. This must be replenished on the expansion time scale  $r/c_s \approx 240 \text{ yr}$ , implying the existence of a reservoir of neutral material, most likely

a disk associated with a low mass star. If the source with a mass loss rate  $10^{-6} M_{\odot} \text{ yr}^{-1}$  is  $10^4$  years old, then  $1 \times 10^{-2} M_{\odot}$  has been lost today, comparable to the disk masses around YSOs.

In principle, the source of material could be an isolated molecular globule but we can place improbable constraints on its mass  $M$ , as follows. First, the clump must be sufficiently bound by self gravity to avoid disruption by the tidal field of Sgr A\*. At distance  $d$  from Sgr A\*, this implies that its density exceeds the Roche density, i.e.  $n_{\text{H}} \gtrsim 10^8 (d/\text{pc})^{-3} \text{ cm}^{-3}$ . Second, models of photoevaporative flows (e.g., Störzer & Hollenbach 1990) show that heating by FUV photons drives a neutral wind from the surface that reaches escape speed before being ionized by EUV photons at a somewhat larger radii. Thus the neutral material passes through a sonic point at some radius  $r \lesssim 500$  AU. At this point the flow speed, sound speed, and escape velocity  $\sqrt{2GM/r}$  are all equal, so we can obtain an estimate for the total mass inside the sonic surface by noting that the sound speed in the warm atomic wind will be  $\sim 3 \text{ km s}^{-1}$  (corresponding to  $\sim 1500 \text{ K}$ ), yielding  $M \approx 0.5 r_{100} M_{\odot}$ , and mean density inside the sonic point  $\langle n_{\text{H}} \rangle \approx 3 \times 10^{10} r_{100}^{-2} \text{ cm}^{-3}$ , where  $r_{100} = r/(100 \text{ AU}) \lesssim 5$ . As such a dense and massive globule would collapse and form a YSO, it is therefore much more plausible that the reservoir of neutral material is instead a circumstellar disk, with  $M$  being dominated by the central star.

There is further evidence for current star formation activity in the E arm from ALMA observations which detected 11 unresolved sources of SiO (5-4) line emission within 0.5 pc of Sgr A\* (Yusef-Zadeh et al. 2013). The SiO sources were interpreted as highly embedded protostellar outflows with typical mass of swept up molecular gas  $\sim 0.2 M_{\odot}$ . We searched for additional SiO emission from the data published earlier (Yusef-Zadeh et al. 2013) and found a weak SiO source 12 toward the cluster of proplyds. Figure 3a shows the positions of SiO (5-4) sources 4 and 5 (Yusef-Zadeh et al. (2013) and the new source 12, drawn as ellipses, superimposed on a grayscale continuum image at 34 GHz. Figure 3b shows the spectrum of the new SiO source 12 at  $(\alpha, \delta) = 17^{\text{h}}45^{\text{m}}41^{\text{s}}.36, -29^{\circ}0'24''.57$ . A Gaussian fit to this spectrum gives peak flux density  $13.69 \pm 1.81 \text{ mJy beam}^{-1}$  corresponding to SiO luminosity  $\sim 4 \times 10^{-6} L_{\odot}$ . We note that the SiO (5-4) sources 4, 5 and 12 coincide with the concentration of proplyds candidates. The parameters of the fitted spectra of SiO (5-4) sources 4, 5 and 12 show central velocities  $\sim 8, 14$  and  $36 \text{ km s}^{-1}$  and total linewidths of  $\sim 25, 18$  and  $54 \text{ km s}^{-1}$  respectively. These characteristics are very similar to those found in low mass protostellar outflows found in the Galactic disk (Gibb et al. 2004; Yusef-Zadeh et al. 2013). The presence of proplyd candidates in the vicinity of SiO (5-4) source is consistent with this interpretation, signifying that low mass star formation near Sgr A\* has occurred within the last  $10^4 - 10^5$  years.

We also searched for near-IR counterparts to the radio sources and placed a  $1\sigma$  upper limit of  $8.6 \mu\text{Jy}$  at  $3.8 \mu\text{m}$  for most sources. This population differs from the recently reported 44 GHz sources (Yusef-Zadeh et al. 2014) and the near-IR identified bow-shock sources (Tanner et al. 2005; Sanchez-Bermudez et al. 2014) in that they do not have bright near-IR counterparts. We can not find near-IR stellar counterparts to radio sources listed in Table 1 with certainty because of the lack of stellar proper motion data and confusing sources in

this region. Two exceptions are proplyd candidates P7 and P8 which appear to have weak  $3.8 \mu\text{m}$  counterparts at a level of  $\sim 20 \mu\text{Jy pixel}^{-1}$ . The near-IR luminosity is estimated to be  $4 \times 10^{-2} L_{\odot}$  using  $4 \pi d^2 \times \nu S_{\nu}$  where the flux density  $S_{\nu} \sim 3\sigma$  from a pixel size of  $\sim 200$  AU (25 mas). Most of the energy from an embedded star and the disk emerges in the far-IR and millimeter parts of the spectrum. Future high resolution observations of these sources should provide better constraints on the luminosity of the proplyd candidates.

#### 4. Discussion

We report the detection of 44 partially resolved radio continuum sources with typical sizes of  $\sim 300\text{-}1000$  AU. We interpret the newly detected cluster of radio sources as a population of proplyd-like objects, implying that low mass star formation is presently taking place in the Galactic center.

First, the radio sources display a bow-shock morphology facing the luminous stars located at the Galactic center. The second line of argument is the lack of luminous near-IR counterparts to radio sources is consistent with an embedded low mass star. Like other star forming regions in the Galaxy where proplyds are detected with tear-shaped geometry or a disk silhouetted against the background radiation, the emission from radio proplyds as well the shape and size of proplyds are consistent with being photoevaporated from a gaseous disk by the FUV radiation and then photoionized by the EUV Lyman continuum radiation from hot stars in the inner 0.4 pc of the Galaxy (Johnstone et al. 1998; Störzer and Hollenbach 1999). In addition, there is a lack of correlation between the luminosity and velocity linewidths of SiO (5-4) line emission from the region where the cluster of proplyd-like objects (RC1) is detected. The relationship is consistent with that found in low mass star formation in the disk of the Galaxy.

Third the proplyd candidates lie at the edge of an elongated molecular cloud which provides a reservoir of gas that feeds star formation activity. The morphology of ionized gas in the E arm (Fig. 1a) suggests that an elongated molecular cloud with an extent of  $20'' \times 5''$  lies within the inner pc of the Sgr A\*. Proplyd candidates are likely produced from this cloud. Support for this suggestion comes from the presence of a radio dark cloud (RDC) associated with the E arm. The dark elongated feature in Fig. 1 is completely surrounded by the ionized gas associated with the E arm. A neutral gas cloud embedded within a bath of radiation field of the Galactic center suppresses radio continuum emission from the interior of the cloud but is edge brightened. The dark feature within the E arm is anti-correlated with  $\text{H}_2$  emission detected at  $2.12 \mu\text{m}$  (Fig. 5f of Yusef-Zadeh 2012). There is also the appearance of a small dark feature near RC2 but needs to be confirmed in future molecular line observations. The presence of radio dark clouds implies that there is a supply of dense gas where the proplyds candidates are detected, thus feeding star formation activity near Sgr A\*. Figure 4 shows a schematic diagram of the radio cloud sandwiched between the ionized gas associated with the E arm and the cluster of proplyd-like objects (RC1) formed at the northern edge of the cloud. The large-scale bow-shock sources to the south of the E arm (Fig. 1a) could belong to the class of EGGs similar to sources seen in M16 (e.g., Hester et al. 1996).

In order for gas clouds near Sgr A\* to collapse and form stars, two conditions must be met. One is that self-gravity must overcome the strong tidal shear of Sgr A\* such that the density of the gas  $n_{\text{H}}$  has to be greater than  $2 \times 10^8 (d/1\text{pc})^{-3} \text{ cm}^{-3}$ . The other is that the cloud mass exceeds the Jeans mass  $M_J = 1.5 (T/100\text{K})^{3/2} (n/10^8 \text{ cm}^{-3})^{-1/2} M_{\odot}$ . The combination of these two conditions give  $M_J > 1 (d/1\text{pc})^{3/2} (T/100\text{K})^{1.5} M_{\odot}$ . Assuming that the gas density is sufficiently high, this suggests that the low mass stars are preferentially formed within a few arcseconds of Sgr A\* with the implication that the IMF may be bottom heavy. The young stars with  $5'' - 10''$  of Sgr A\* are reported to have a top-heavy IMF (Bartko et al. 2010, Lu et al. 2013). If clumps with Jeans mass contract and sub-fragment, then a population of brown dwarfs are expected to lie close to Sgr A\*. An additional implication of low mass star formation near Sgr A\* is that protoplanetary objects in the FUV dominated region have lower mass-loss rates, perhaps could retain sufficient disk mass to allow potential planetary formation (Mann et al. 2014).

In conclusion, we presented new radio images of the Galactic center and showed 44 compact radio sources within the E arm. Radio sources with near-IR counterparts are thought to be massive young stellar objects (Yusef-Zadeh et al. 2014) whereas radio sources without any infrared counterparts are likely associated with protoplanets around low mass stars. We also showed that star formation is taking place at the edge of an elongated neutral cloud, represented as a dark feature in a continuum image at 34 GHz as well as being traced by  $\text{H}_2$  emission. The southern edge of the RDC traces the E arm of Sgr A West, photoionized by the strong radiation field of the Galactic center whereas the northern edge of the RDC signifies low mass star formation activity. Future mid-IR and millimeter observations should conclusively test whether protoplanets lie close to Sgr A\* and potentially measure the disk mass of Galactic center protoplanet-like objects.

Acknowledgments: This work is partially supported by the grant AST-0807400 from the NSF, DPO986386 from the Australian Research Council and the European Research Council under the European Union’s Seventh Framework Program (FP/2007-2013). This paper makes use of the following ALMA data: ADS/JAO.ALMA#2011.0.00005.SV. ALMA is a partnership of ESO (representing its member states), NSF (USA) and NINS (Japan), together with NRC (Canada) and NSC and ASIAA (Taiwan), in cooperation with the Republic of Chile. The Joint ALMA Observatory is operated by ESO, AUI/NRAO and NAOJ. The research leading to these results has received funding from ERC Grant Agreement n. 614922.

## REFERENCES

- Bartko, H., Martins, F., Trippe, S., et al. 2010, *ApJ*, 708, 834
- Churchwell, E., Felli, M., Wood, D. O. S. et al. 1987, *ApJ*, 321, 516
- Eckart, A., Muzic, K., Yazici, S. et al. 2013, *A&A*, 551, 18
- Garay, G., Moran, J. M. & Reid, M. 1987, *ApJ*, 314, 535
- Genzel, R., Eisenhauer, F., & Gillessen, S. 2010, *Reviews of Modern Physics*, 82, 3121

- Genzel, R., Hollenbach, D. & Townes, C. H. 1994, *Reports on Progress in Physics*, 57, 417
- Ghez, A. M., Salim, S., Weinberg, N. N. et al. 2008, *ApJ*, 689, 1044
- Gibb, A. G., Richer, J.S., Chandler, C.J., & Davis, C. J. 2004, *ApJ*, 603, 198
- Gillessen, S., Eisenhauer, F., Trippe, S. et al. 2009, *ApJ*, 692, 1075
- Hester, J. J., Scowen, P. A., Sankrit, R. et al. 1996, *AJ*, 111, 2349
- Horrobin, M., Eisenhauer, F., Tecza, M. et al. 2004, *Astronomische Nachrichten*, 325, 2, 88
- Johnstone, D., Hollenbach, D. & Bally, J. 1998, *ApJ*, 499, 758
- Kennea, J. A., Burrows, D. N., Kouveliotou et al. 2013, *ApJ*, 770, L24
- Lu, J. R., Ghez, A. M., Hornstein, S. D. et al. 2009, *ApJ*, 690, 1463
- Lu, J. R., Do, T., Ghez, A. M. et al. 2013, 764, 155
- Mann, R. K., Di Francesco, J., Johnstone, D. et al. 2014, *ApJ*, 784, 82
- Muzic, K., Schödel, R., Eckart, A., Meyer, L. & Zensus, A. 2008, *A&A*, 482, 173
- O'Dell, C. R. & Wen Z. 1994, *ApJ*, 436, 194
- Paumard, T., Genzel, R., Martins, F. et al. 2006, *ApJ*, 643, 1011
- Pott, J., Eckart, A., Glindemann, A. et al. 2005, *Messenger*, 119, 43
- Reid, M. J. & Brunthaler, A. 2004, *ApJ*, 616, 872
- Sanchez-Bermudez, J., Schödel, R., Alberdi, A., et al. 2014, *A&A*, 567, AA21
- Serabyn, E., Lacy, J. H. & Achtermann, J. M. 1991, *ApJ*, 378, 557
- Schödel, R., Najarro, F., Muzic, K. & Eckart, A. 2010, *A&A*, 511, 18
- Schödel, R., Yelda, S., Ghez, A. et al. 2013, *MNRAS*, 429, 1367
- Smith, N., Bally, J. & Morse, J. A. 2003, *ApJ*, 587, L105
- Störzer, H. & Hollenbach, D. 1998, *ApJ*, 515, 669
- Tanner, A., Ghez, A. M., Morris, M. R. & Christou, J. C. 2005, *ApJ*, 624, 742
- Viehmann, T., Eckart, A., Schödel, et al. 2006, *ApJ*, 642, 861
- Yusef-Zadeh, F., Biretta, J. & Geballe, T. R. 2005, *AJ*, 130, 117
- Yusef-Zadeh, F., Roberts, D. A., Bushouse, H. A. et al. 2014, *ApJ*, 792, 1
- Yusef-Zadeh, F., Royster, M., Wardle, M. et al. 2013, *ApJ*, 767, L32

Yusef-Zadeh, F. 2012, ApJ, 759, L11

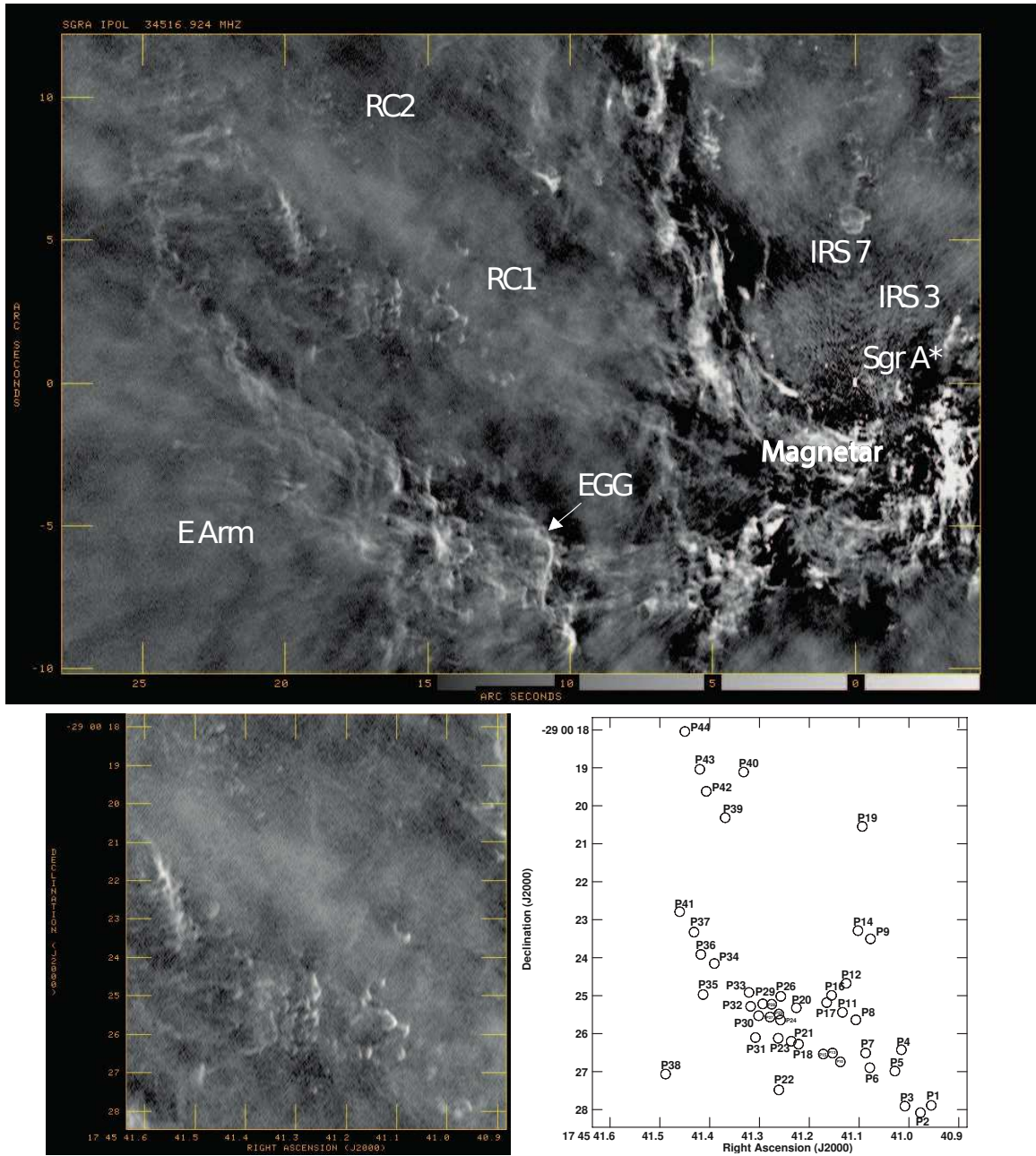


Fig. 1.— (a) The prominent N and E arms of Sgr A West and the proplyd candidates (RC1 & RC2) and an evaporating gaseous globule EGG candidate at 34 GHz. (b) The same as (a) except a close up view of proplyd candidates. (c) ID numbers of of proplyd candidates (Table 1) are labeled over an identical region shown in (b).

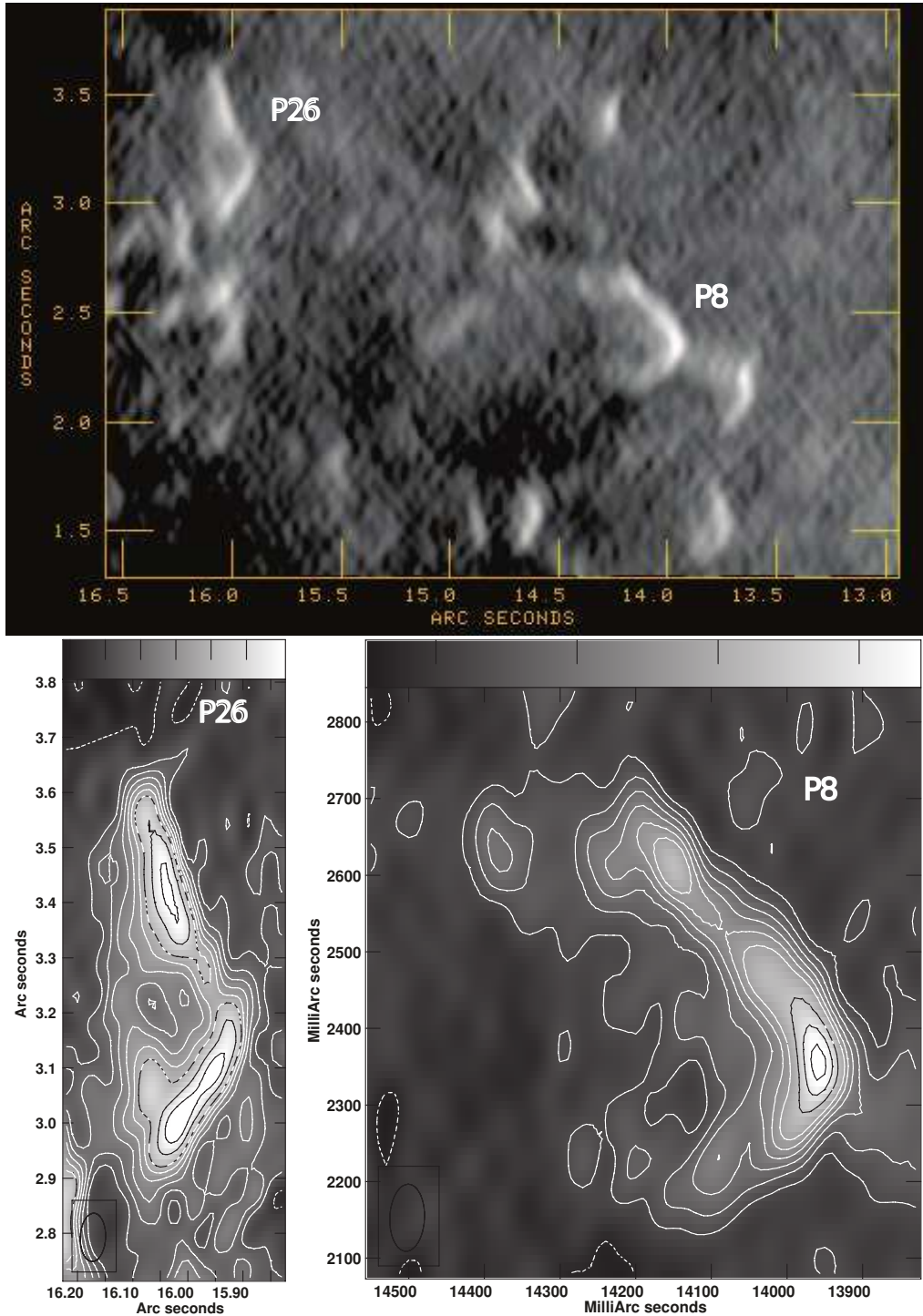


Fig. 2.— (a) A  $3.5'' \times 2.5''$  of a 34 GHz image showing a concentration of proplyd candidates offset by  $15''.2$  NE of Sgr A\*. (b) Grayscale contours of P26 are set at  $-10, 10, 20, \dots, 60, 80, \dots, 120 \mu\text{Jy beam}^{-1}$ . (c) Grayscale contours of P8 are set at  $-10, 10, 20, \dots, 60, 80$  and  $100 \mu\text{Jy beam}^{-1}$ .

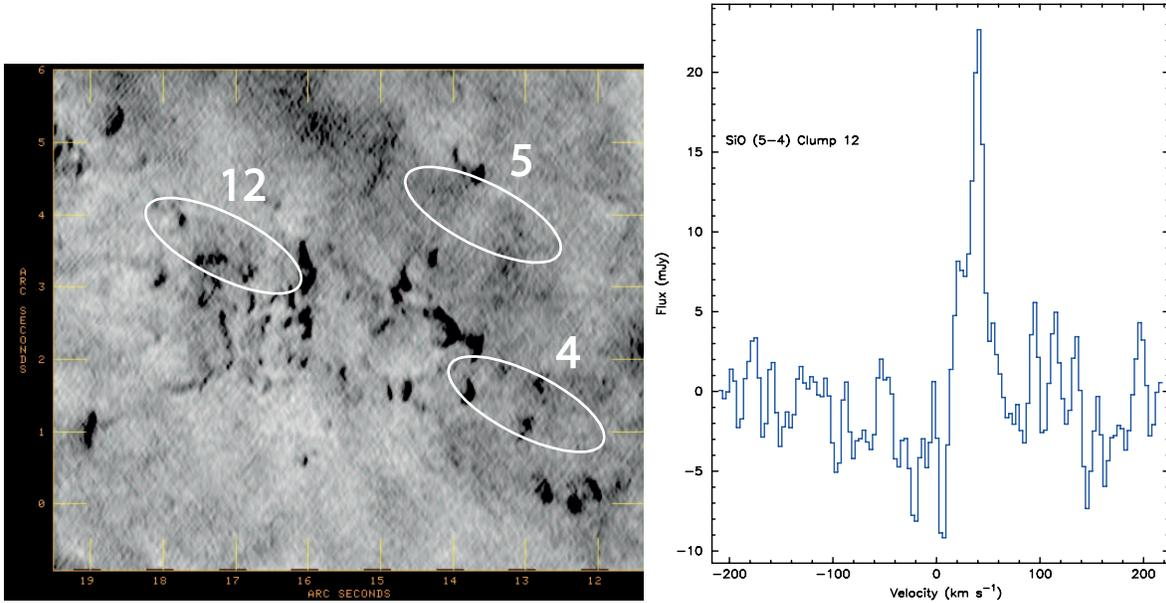


Fig. 3.— (a) Three ellipses corresponding to the location of three SiO (5-4) sources 4, 5 and 12 are drawn on a 34 GHz grayscale image (reverse color) of proplyd-like objects. (b) The ALMA spectrum of source 12. The size and position angle of each ellipse corresponds to the spatial resolution of ALMA data (Yusef-Zadeh et al. 2013).

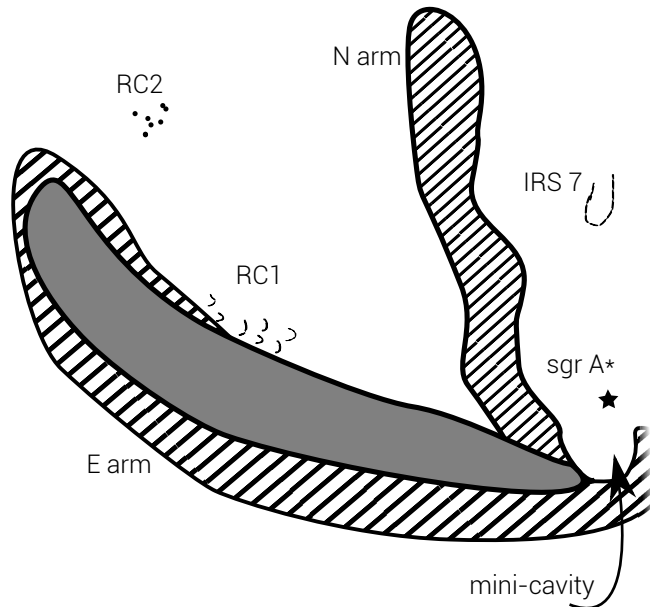


Fig. 4.— A schematic view of the region shown in Figure 1a. Shaded region coincides with radio dark clouds where hashed lines trace the distribution of ionized gas associated with the E and N arms of Sgr A West.

Table 1. The Parameters of Gaussian Fitted 34 GHz Sources

ID	RA (J2000) (17 <sup>h</sup> 45 <sup>m</sup> )	Dec (J2000) (−29°00′)	Dist. from Sgr A* (arcsec)	Pos. Accuracy (mas)	$\theta_a \times \theta_b$ (PA) mas $\times$ mas (deg)	Peak Intensity (mJy beam <sup>−1</sup> )	Integrated Flux (mJy)
P1	40.9554	27.8883	12.03	17.15	242 $\times$ 54 (27)	0.077 $\pm$ 0.013	0.376 $\pm$ 0.077
P2	40.9770	28.0816	12.31	18.76	198 $\times$ 155 (25)	0.062 $\pm$ 0.013	0.531 $\pm$ 0.124
P3	41.0083	27.9076	12.73	27.53	360 $\times$ 194 (19)	0.053 $\pm$ 0.010	0.961 $\pm$ 0.184
P4	41.0153	26.4246	12.92	32.41	154 $\times$ 86 (5)	0.031 $\pm$ 0.013	0.131 $\pm$ 0.068
P5	41.0284	26.9837	13.03	30.20	339 $\times$ 199 (159)	0.046 $\pm$ 0.010	0.812 $\pm$ 0.181
P6	41.0787	25.8970	13.82	8.61	169 $\times$ 46 (172)	0.126 $\pm$ 0.013	0.383 $\pm$ 0.053
P7	41.0871	26.5111	13.85	12.51	177 $\times$ 50 (7)	0.090 $\pm$ 0.013	0.298 $\pm$ 0.056
P8	41.1067	25.6379	14.22	17.45	477 $\times$ 77 (38)	0.112 $\pm$ 0.012	1.340 $\pm$ 0.153
P9	41.0773	23.5031	14.37	9.47	170 $\times$ 88 (157)	0.109 $\pm$ 0.013	0.516 $\pm$ 0.075
P10	41.1378	26.7426	14.48	25.61	155 $\times$ 109 (79)	0.031 $\pm$ 0.013	0.170 $\pm$ 0.085
P11	41.1336	25.4366	14.61	15.48	103 $\times$ 58 (40)	0.046 $\pm$ 0.014	0.123 $\pm$ 0.048
P12	41.1260	24.6733	14.67	8.26	132 $\times$ 42 (168)	0.110 $\pm$ 0.014	0.269 $\pm$ 0.045
P13	41.1535	26.5116	14.71	10.70	212 $\times$ 66 (168)	0.119 $\pm$ 0.013	0.539 $\pm$ 0.072
P14	41.1024	23.2867	14.76	34.42	255 $\times$ 57 (11)	0.043 $\pm$ 0.013	0.213 $\pm$ 0.077
P15	41.1722	26.5353	14.95	16.37	186 $\times$ 25 (11)	0.071 $\pm$ 0.014	0.195 $\pm$ 0.049
P16	41.1555	24.9915	14.98	12.71	229 $\times$ 58 (20)	0.103 $\pm$ 0.013	0.480 $\pm$ 0.074
P17	41.1652	25.1813	15.06	13.94	189 $\times$ 82 (9)	0.083 $\pm$ 0.013	0.400 $\pm$ 0.075
P18	41.2218	26.2771	15.63	29.23	235 $\times$ 91 (5)	0.048 $\pm$ 0.013	0.298 $\pm$ 0.094
P19	41.0938	20.5442	15.76	37.64	208 $\times$ 91 (179)	0.033 $\pm$ 0.013	0.187 $\pm$ 0.086
P20	41.2261	25.3190	15.82	1.19	83 $\times$ 38 (75)	0.482 $\pm$ 0.014	1.062 $\pm$ 0.042
P21	41.2364	26.1998	15.83	27.52	105 $\times$ 37 (12)	0.029 $\pm$ 0.014	0.059 $\pm$ 0.039
P22	41.2612	27.4809	16.05	12.60	99 $\times$ 34 (168)	0.061 $\pm$ 0.014	0.116 $\pm$ 0.038
P23	41.2625	26.1203	16.08	14.97	113 $\times$ 46 (140)	0.049 $\pm$ 0.014	0.126 $\pm$ 0.046
P24	41.2580	25.6416	16.18	18.90	268 $\times$ 66 (168)	0.082 $\pm$ 0.013	0.459 $\pm$ 0.086
P25	41.2612	25.4816	16.25	6.93	64 $\times$ 28 (139)	0.088 $\pm$ 0.014	0.140 $\pm$ 0.034
P26	41.2573	25.0159	16.28	12.98	231 $\times$ 27 (148)	0.094 $\pm$ 0.013	0.363 $\pm$ 0.063
P27	41.2789	25.5619	16.47	11.17	154 $\times$ 36 (135)	0.073 $\pm$ 0.013	0.230 $\pm$ 0.054
P28	41.2756	25.2243	16.48	20.27	259 $\times$ 37 (4)	0.076 $\pm$ 0.013	0.302 $\pm$ 0.065
P29	41.2935	25.2169	16.71	23.66	265 $\times$ 51 (136)	0.050 $\pm$ 0.013	0.285 $\pm$ 0.086
P30	41.3018	25.5289	16.77	13.65	144 $\times$ 63 (143)	0.062 $\pm$ 0.013	0.217 $\pm$ 0.058
P31	41.3083	26.1015	16.78	13.89	80 $\times$ 23 (28)	0.049 $\pm$ 0.014	0.081 $\pm$ 0.034
P32	41.3180	25.2808	17.02	28.45	254 $\times$ 78 (177)	0.053 $\pm$ 0.013	0.313 $\pm$ 0.090
P33	41.3212	24.9135	17.12	26.66	229 $\times$ 57 (134)	0.039 $\pm$ 0.013	0.205 $\pm$ 0.081
P34	41.3907	24.1522	18.17	18.15	174 $\times$ 83 (11)	0.060 $\pm$ 0.013	0.272 $\pm$ 0.072
P35	41.4134	24.9705	18.30	23.68	232 $\times$ 107 (150)	0.053 $\pm$ 0.013	0.384 $\pm$ 0.107
P36	41.4180	23.9140	18.57	32.84	188 $\times$ 87 (175)	0.035 $\pm$ 0.013	0.177 $\pm$ 0.078
P37	41.4316	23.3262	18.88	42.84	218 $\times$ 125 (162)	0.030 $\pm$ 0.013	0.226 $\pm$ 0.112
P38	41.4885	27.0644	19.05	28.39	441 $\times$ 145 (168)	0.066 $\pm$ 0.010	1.105 $\pm$ 0.177
P39	41.3689	20.3132	19.10	21.94	179 $\times$ 52 (119)	0.034 $\pm$ 0.013	0.146 $\pm$ 0.069
P40 <sup>a</sup>	41.3320	19.1091	19.19	17.19	121 $\times$ 1 (138)	0.043 $\pm$ 0.014	0.095 $\pm$ 0.042
P41	41.4604	22.7882	19.39	36.96	385 $\times$ 159 (156)	0.043 $\pm$ 0.010	0.695 $\pm$ 0.174
P42 <sup>a</sup>	41.4068	19.6192	19.84	20.02	144 $\times$ 0 (142)	0.042 $\pm$ 0.014	0.090 $\pm$ 0.041
P43	41.4199	19.0363	20.25	22.69	140 $\times$ 17 (143)	0.036 $\pm$ 0.014	0.090 $\pm$ 0.045
P44	41.4499	18.0418	21.06	18.59	227 $\times$ 122 (119)	0.053 $\pm$ 0.013	0.439 $\pm$ 0.120

<sup>a</sup>spatially unresolved in one direction